High-Resolution Interrogation Technique for Fiber Bragg Grating Sensor Using Long-Period Fiber Grating Pair and Erbium-Doped Fiber

Jaehoon Jung, Yong Wook Lee, and Byoungho Lee*

School of Electrical Engineering, Seoul National University, Seoul 151-744, KOREA

A novel interrogation scheme to detect fine Bragg wavelength shift using a long period fiber grating pair with erbium-doped fiber inserted between the two gratings is reported. The technique is shown to feature high resolution and much more immunity to temperature perturbation compared to the conventional Mach-Zehnder interferometer demodulation system. For quasi-static strain measurement, this approach provides high wavelength resolution of 0.05 pm that corresponds to 41.7 nϵ in strain and 3.8×10^{-3}°C in temperature. This interrogation system is also employed in dynamic measurement to obtain the minimum detectable strain perturbation of ~ 8.76 nϵ/Hz$^{1/2}$ at 100 Hz. Moreover, this interrogation system has prominent thermal stability. This thermal stability comes from the fact that two arms of the interferometer, the core and cladding in erbium-doped fiber, are exposed to nearly the same environment.

OCIS codes : 060.2370, 060.2410.

I. INTRODUCTION

Wavelength interrogation for fiber-optic sensor based on fiber Bragg grating (FBG) has been an active research field. It is essential to develop a suitable scheme that translates the wavelength-encoded signal into a corresponding signal more amenable to conventional electronic processing. For temperature and strain detection, the precision of the Bragg grating wavelength shift is crucial to achieving good sensor performance. Many techniques have been proposed based on fiber edge filters [1], tunable fiber Fabry-Perot filters [2], and tunable acoustooptic filters [3]. Although these schemes have some advantages, they do not have sufficient resolution to detect fine wavelength shifts. For high-resolution wavelength detection, interferometric wavelength discrimination can be used by employing a piezoelectrically tuned, unbalanced Mach-Zehnder interferometer (MZI). The MZI filter has provided high-resolution wavelength-shift detection with large bandwidth in FBG interrogation [4]. It needs, however, either a complete temperature-isolation process or the insertion of a reference grating to avoid the temperature perturbation at the MZI wavelength shift discriminator, because the MZI is so sensitive to the ambient temperature that an interfer-

ence signal output drifts slowly with time. Recently, a very promising approach was discovered which is shown to operate as a wavelength-dependent amplifying interferometer (WDAI) with the characteristics of high resolution and prominent thermal stability [5], [6]. The WDAI which consists of a long period fiber grating (LPG) pair with erbium-doped fiber (EDF) inserted between the two gratings was employed to detect fine Bragg wavelength shift. The proposed technique showed high wavelength-resolution compared to the MZI demodulation system.

In this paper, we demonstrate its adoptability in dynamic measurements as well as in quasi-static ones and we test the thermal stability. The experimental results show that the WDAI has wavelength resolution of 0.05 pm for quasi-static perturbation and is applicable to fast dynamic measurement with good system sensitivity. The experimental results to demonstrate thermal stability are also presented.

II. PRINCIPLE OF OPERATION

The fiber MZI based on two 3dB wavelength division multiplexers (WDM) is successfully used to solve many physical tasks, for example, measuring the induced refractive index in the fiber core [7]. Phase

change in one of the interferometer's arms leads to a corresponding change in the interference signal at the fiber output. Such an interferometer is applicable in a variety of high-resolution measurements, but has significant drawbacks. Because the fiber arms are rather long, the operating temperature must be well stabilized. As a rule, a laser with a high coherence length must be used as the light source, or the interferometer arms' lengths must be equalized with high precision.

Dianov et al. proposed a new type of MZI based on two cascaded-LPGs [8]. In this new device, optical path difference exists in the core and cladding of the optical fiber instead of in two different arms as in conventional MZI. While the light propagating along the different optical paths in the conventional MZI experiences different environments, such as temperature and hence refractive index, the light propagating in core and cladding for the cascaded LPG structure experiences negligible dissimilar temperature. Thus, the two-cascaded LPG interferometer does not feature the above-mentioned disadvantages and can be used for many practical purposes. LPG pairs have been studied as sensor elements and telecommunication devices [9]- [11].

If the incident light in the first LPG satisfies the phase matching condition, the light is coupled to the cladding mode. The phase matching condition between the guided mode and a forward propagating cladding mode is given by

$$\beta_{core} - \beta_{clad} = 2\pi/\Lambda, \qquad (1)$$

where Λ is the grating period, and β_{core} and β_{clad} are the propagation constants of core mode and cladding mode, respectively. The cladding mode coupled by the front grating is recoupled into the core by the following grating, which produces a series of interference fringes in the corresponding stop band of the single LPG.

We proposed a novel device (WDAI) that consists of an LPG pair and EDF inserted between the two gratings [5], [6]. In the device, shown in Fig. 1, when pumped, the propagating beam in the core of EDF is amplified during the trip to the second grating. Incident broadband lights are amplified by an amount depending on the coupling at the first grating. After the first grating, the out-coupled light propagates in the cladding without amplification and the remaining light propagating in the core is amplified. When the two lights, in the core and cladding, meet the second LPG, they are recoupled by the grating and the interference fringes in the wavelength domain appear behind the second grating. The magnitude of interference output depends not only on the wavelength but also on the amplification by the EDF.
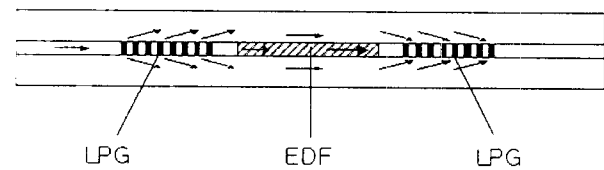

FIG. 1. Schematic diagram of wavelength-dependent amplifying interferometer consisting of long period fiber grating pair and erbium-doped fiber inserted between the two gratings. LPG: long period fiber grating, EDF: erbium-doped fiber.

When pumping the EDF, the more light is left in the core, the larger the amplification is under the high pump condition. Let us assume that we pump the EDF of the WDAI in a sinusoidal form and use this 'modulated' light as the light source for an FBG sensor. When the measurand such as temperature or strain is fixed, the light reflected by the FBG stays at some wavelength. The signal at the photodetector for the returned light contains 'modulated' light signal, i.e., the component at the modulation frequency. Thus, by measuring the photocurrent value at the modulation frequency, we interrogate the wavelength of the signal and hence, the physical measurand. That is, if we modulate the pump current in a sinusoidal pattern, the amplitude of the fundamental harmonic component is wavelength-dependent. Furthermore, dynamic perturbation also could be monitored provided that the modulation frequency of the EDF exceeds the variation frequency of the strain or temperature to be measured. Therefore, by the pseudo-heterodyne method, the reflected wavelength of the FBG can be interrogated.

Consider the transmission power of the WDAI and optical gain with pumping as shown in Fig. 2. Note that the peaks in the transmission spectrum turn out
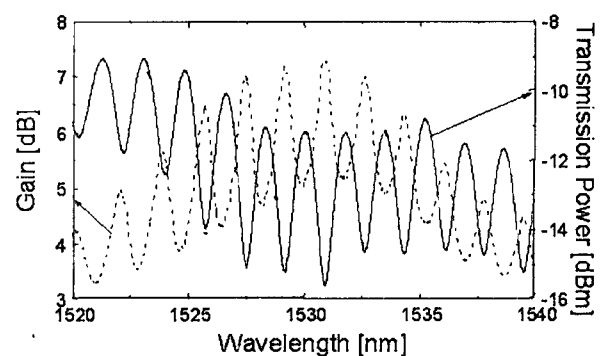

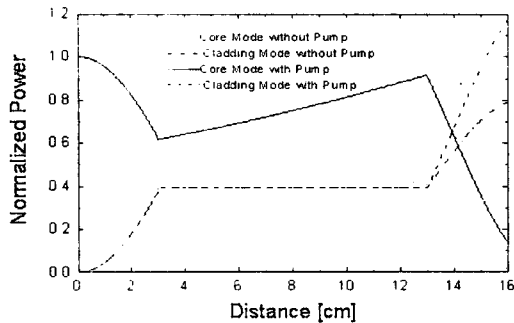FIG. 2. Transmission power of the WDAI and optical gain with puming.

FIG. 3. Propagation along the WDAI in case of destructive interference.

FIG. 4. Propagation along the WDAI in case of constructive interference.

to be the dips in the gain and vice versa. Figs 3 and 4 show the calculated power of propagating light along the device at wavelength around dip (destructive) and peak (constructive interference), respectively. In Figs. 3 and 4, the core mode was about half out-coupled and still decreasing at the end of the first grating. For this case, when the phase variation (that the light experiences in the region of EDF) is additive to one at the end of the first grating, that is, when 'decrease state' in core mode still remains after propagation, the destructive interference occurs as shown in Fig. 3. Thus, the light at this wavelength is located around a dip in transmission spectrum. The optical gain (10 log [(Power with pump)/(Power without pump)]) is rather larger in this case than that in 'constructive' case since the power of light is very small, nearly around zero before amplification. In the constructive case, although optical power difference has a larger value, the gain is smaller than in the destructive case. There are slight mismatches in positions of peaks and dips in Fig. 2, which result from the pump-induced change in the refractive index.

III. EXPERIMENTS AND DISCUSSIONS

Two cascaded, nearly identical LPGs, each with length of 3 cm, were written onto normal single-mode communication fibers with hydrogen loading and a 10 cm-long EDF was fusion-spliced between the two gratings. The LPGs were fabricated by irradiation of the fiber core with 248 nm KrF laser light through an amplitude mask, which induces a periodic refractive index modulation along the fiber axis in hydrogen-loaded germanosilicate fibers. The grating period was 500 μm, and the duty cycle of the refractive index modulation was 50 %. To obtain the same gratings, the irradiation time was controlled so that the trans-
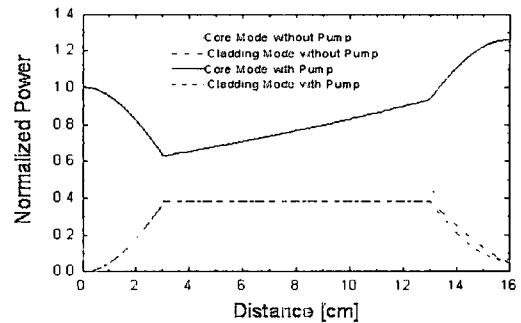
mission dip and the resonant wavelength were identical. The energy density of the laser irradiation was $\sim$ 250 mJ/cm^2 per pulse. In the case of an LPG pair with different transmission spectra, the amount of coupling between two modes at the second LPG is different from that at the first LPG. For example, when the larger coupling at a wavelength happens in the first LPG, the cladding mode propagating along the cladding of the EDF cannot be recoupled to the core fully at the second LPG and the remnant light in the cladding becomes a transmission loss. On the contrary, when the smaller coupling at a wavelength occurs initially, the full coupling happens at a point in the second grating and after that, the coupling from the core to the cladding mode begins again, which results in a transmission loss. Consequently, when two gratings have different transmission dips, the lights suffer from insertion loss even in constructive interference.

Fig. 5 shows the schematic diagram for our experiment. Broadband source light was launched into the WDAI and modulated by input current of the pump LD (Lasertron QLMSS 470-311). A light at Bragg wavelength was reflected at the FBG and coupled into the photodetector (Newport 818-BB-31). The photocurrent signal at the photodetector enters the lock-in amplifier (SRS 830) for low-noise detection of the
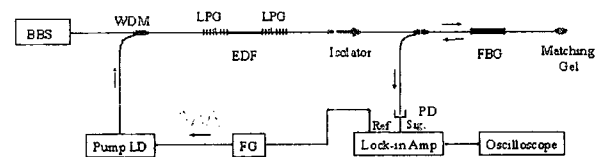

FIG. 5. Experimental setup. BBS: broadband source. WDM: wavelength division multiplexing coupler. LD: laser diode, FG: function generator, PD: photodetector.
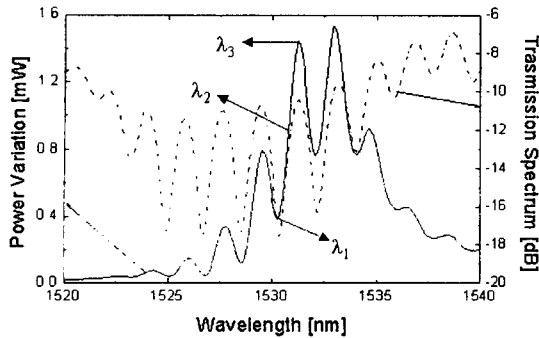
FIG. 6. The transmission spectrum (without LD pumping) of the device used in this experiment and the difference in optical transmission power without and with pump power of 90 mW.

first harmonic component.

The transmission spectrum of the device (without LD pumping) used in this experiment and the linear-scale difference in optical transmission power (without and with pump power of 90 mW) are shown in Fig. 6. The peaks of the fringes in Fig. 6 do not reach 0 dB and this loss may come from the following three factors. The first is the loss caused by the outer coating in the region where the cladding mode exists. In practice, the coating interface is a main source of power loss in the cladding mode. Hence, although two LPGs are identical, the coupled-out mode in the cladding may not come fully into the core. The second one comes from the fact that this device consists of two dissimilar fibers (single mode fiber and EDF) and hence their corresponding cladding modes are not the same. The cladding mode in the single mode fiber onto which LPG is written suffers from power loss since it does not match that in EDF exactly. The last factor is EDF absorption loss. It is expected that the light propagating in the EDF experiences some loss since the EDF absorbs the light in the case of no pumping. Pumping EDF inserted between two LPGs by a sinusoidal pattern produces the modulation of light launched into the FBG, and the fundamental harmonic component amplitude is proportional to the change in optical power shown in Fig. 6.

1. Quasi-Static Strain Measurement

We used the device whose transmission was shown in Fig. 6 to interrogate an FBG strain sensor system. The input current of the pump LD was modulated by a sinusoidal pattern with peak pump power of 90 mW. To induce a quasi-static strain in the FBG,

we attached both ends of the FBG to the translation mounts and introduced test strains by applying a known test displacement, using a micrometer. The sensor grating (FBG) has nominal Bragg wavelength of 1530.1 nm and 3 dB bandwidth of 0.4 nm. The strains were applied to the FBG so that the wavelengths of reflected light by FBG were $\lambda_1(=1530.25\text{nm})$, $\lambda_2(=1530.7$ nm), $\lambda_3(=1531.25$ nm) in Fig. 6, respectively.

Figs. 7(a), (b), and (c) show the signals at the photodetector at the FBG Bragg wavelengths of λ_1, λ_2, λ_3 at 100 Hz, 500 Hz, and 1kHz of EDF modulation, respectively. The results show that in the range between λ_1 and λ_3, the fundamental harmonic component of the modulation frequency has maximum amplitude at λ_3 and minimum at λ_1, as expected from Fig. 6 since the amplitude of the harmonic is proportional to the optical power difference. The rms values are 178.04 (at λ_1), 232.2 (at λ_2), 376.5 mV (at λ_3) at 100Hz, 58.32 (at λ_1), 72.4 (at λ_2), 118.23 mV (at λ_3) at 500Hz, and 21.23 (at λ_1), 25.2 (at λ_2), 42.85 mV (at λ_3) at 1 kHz, respectively. The values of difference between the peaks at λ_1 and λ_3 are 198.46, 59.91, and 21.62 mV (rms) at each modulation frequency. If we define wavelength shift per unit detection step as 'average resolution', the average resolutions of the wavelength in this system at the modulation frequency of 100 Hz are evaluated as 0.05, 0.167, and 0.463 pm by a lock-in amplifier with detection scale of 10 μV. Given the sensitivities of 1.2 pm/$\mu\epsilon$ and 13 pm/°C [12], these wavelength resolutions correspond to 41.7 nϵ, 0.139 $\mu\epsilon$, and 0.385 $\mu\epsilon$ in strain and 3.8 $\times$ 10^{-3}°C, 1.3 $\times$ 10^{-2}°C, and 3.6 $\times$ 10^{-2}°C in temperature, respectively. Such a high resolution results from modulating the source and using a lock-in amplifier at the receiver, so that the spontaneous emission effect that might exist otherwise and other noises are eliminated. The experimental results show that the rms voltage gets lower at higher modulation frequency due to the fact that the excited erbium ions do not respond to the modulated pumping fully at high frequency. One advantage of using WDAI over conventional MZI is the ability to measure a quasi-static perturbation with high resolution without any additional device.

2. Dynamic Strain Measurement

When the grating sensor is employed to monitor the structural strain profile of a smart structure, it may experience a fast varying dynamic perturbation as well as a static or quasi-static one. Therefore, it is important to analyze the dynamic perturbation for exact understanding of the strain source behavior When we use some wavelength determining devices such as an optical spectrum analyzer, the analysis is impossi-
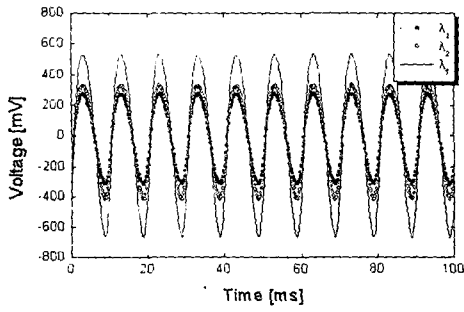
(a)
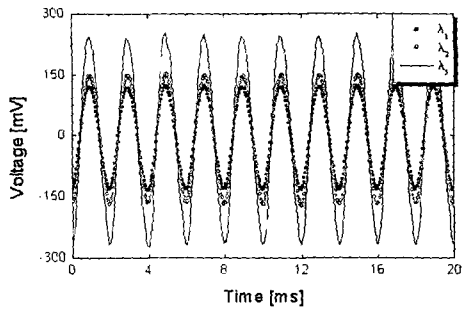
(b)
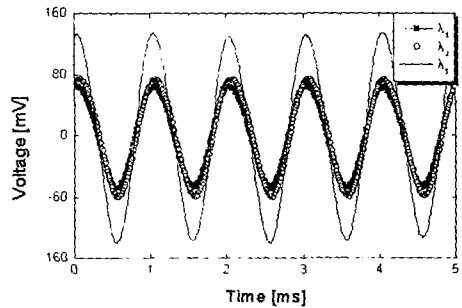
(c)

FIG. 7. (a) Photodetector signals at wavelengths $\lambda_1(=1530.25$ nm), $\lambda_2(=1530.7$ nm), $\lambda_3(=1531.25$ nm), respectively at 100 Hz of EDF modulation, (b) Photodetector signals at wavelengths $\lambda_1(=1530.25$ nm), $\lambda_2(=1530.7$ nm), $\lambda_3(=1531.25$ nm), respectively at 500 Hz of EDF modulation, (c) Photodetector signals at wavelengths $\lambda_1(=1530.25$ nm), $\lambda_2(=1530.7$ nm), $\lambda_3(=1531.25$ nm), respectively at 1kHz of EDF modulation.

ble due to their slow response time. That is because all the bulk-optic spectrometers have to scan the wavelength range with a mechanical grating, which degrades the system performance for a fast varying signal. However, the proposed interferometer is one of the interrogators for dynamic strain measurement.

To induce a known strain signal to the sensor grating, the grating was attached with glue to a fiber stretcher, which introduced a dynamic strain signal

and a function generator output was fed to the PZT inserted between both ends of the fiber stretcher. At first, we performed the measurement of dynamic strain without modulation of pump. To analyze the frequency distribution of the interference output, the signal was fed to the fast-Fourier transform (FFT) network analyzer (SRS 780). Figs. 8(a) and (b) show the photodetector signal and its FFT result of the interferometer output when drive signal of 220 $\mu\epsilon$ (rms) at 1 kHz was applied (dynamic strain). In Fig. 8(b), FFT result is simply the magnitude of the spectrum normalized to a 1 Hz bandwidth. We can clearly see the peak exactly at the PZT drive signal frequency. The signal-to-noise ratio of the 100 Hz was measured as 63.5 dB not in electric power, but in voltage as shown in Fig. 8(b). Therefore, in this case, the minimum detectable strain perturbation is ~ 98.3 pϵ (rms)/Hz$^{1/2}$, which is an ultra-high resolution compared to previous result using MZI [4]. In the case of the sensing scheme without pump modulation, we can obtain an ultrahigh resolution but this is applicable only to dynamic perturbation measurement since non-modulated sig-
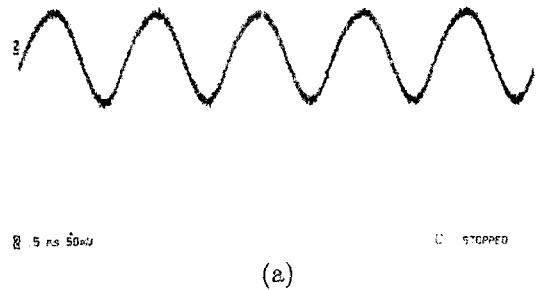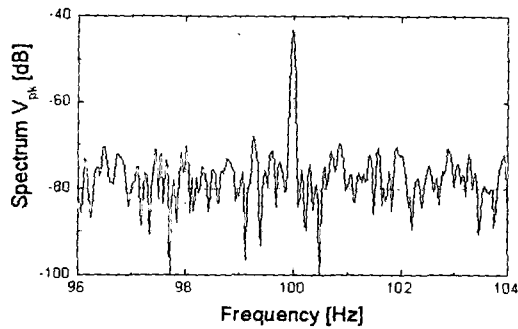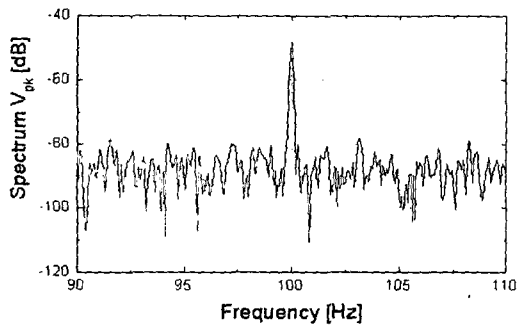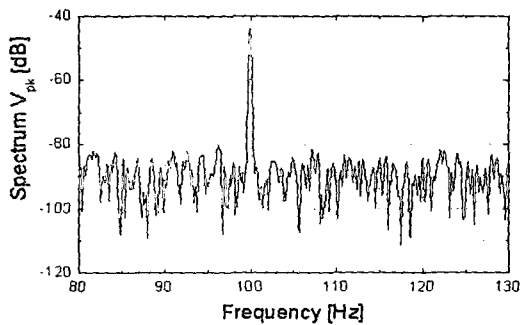

(a)
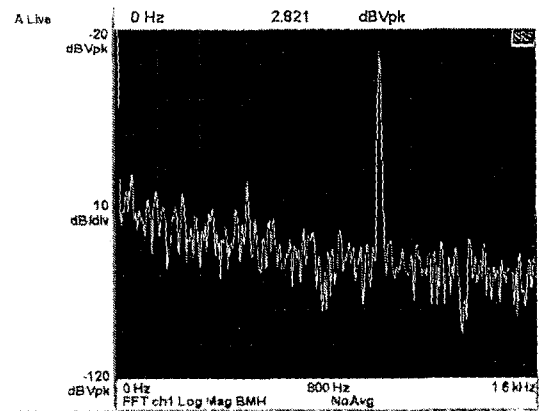
(b)

FIG. 8. (a) Photodetector signal and (b) its FFT result of the interferometer output when drive signal of 220 ϵ (rms) at 1 kHz was applied (dynamic strain).

(a)

(b)

(c)

FIG. 9. (a) FFT voltage spectrum with LD modulation. 220 $\mu\epsilon$ (rms) is applied to the fiber grating at a frequency of 100 Hz with a pump LD modulation frequency of 500 Hz, (b) FFT voltage spectrum with LD modulation. 220 $\mu\epsilon$ (rms) is applied to the fiber grating at a frequency of 100 Hz with a pump LD modulation frequency of 1 kHz, (c) FFT voltage spectrum with LD modulation. 220 $\mu\epsilon$ (rms) is applied to the fiber grating at a frequency of 100 Hz with a pump LD modulation frequency of 5 kHz.

nal might change slowly in intensity.

On the other hand, we measured the dynamic strain with LD modulation. We applied 220 $\mu\epsilon$ (rms) variation to the sensor grating at a frequency of 100 Hz with

a pump modulation frequency of 500 Hz, 1kHz and, 5 kHz to get the effect of modulation frequency on system SNR at a given signal frequency. Figs. 9(a), (b), and (c) show the FFT spectra of the lock-in amplifier outputs. The signal-to-noise ratio of the component was estimated as 44 dB at the modulation frequency of 5 kHz. Therefore in this case, the minimum detectable strain perturbation is $\sim$ 8.76 $n\epsilon/Hz^{1/2}$. Increasing modulation frequency corresponds to more sampling points at a given period and produce better system SNR in case of dynamic measurement. While, for example, at the modulation frequency of 500 Hz the signal at 100 Hz is sampled at 5 points during its period, one at 5 kHz is sampled at 50 points. Therefore, to obtain better system SNR, higher frequency pump modulation is necessary. The modulation frequency, however, cannot be increased without limit since an erbium ion cannot react with the pump at exceedingly high speed. Also, wavelength resolution is degraded as modulation frequency increases, so there is a trade-off between bandwidth and wavelength resolution of this interrogation system.

IV. THERMAL STABILITY

Fig. 10 shows the transmission spectra of the conventional unbalanced MZI, which were measured at different times. The transmission spectrum varied at each measurement and this variation is due to the ambient temperature current. With the random phase fluctuations, the sensor performance for quasi-static perturbations degrades seriously. This demodulation scheme must be used together with another reference grating which experiences the same phase drift [13], or with perfect thermal shielding, which is difficult in practice.

The WDAI has much less (negligible) power drift due to the ambient temperature compared to the conventional unbalanced MZI demodulator. To demon-
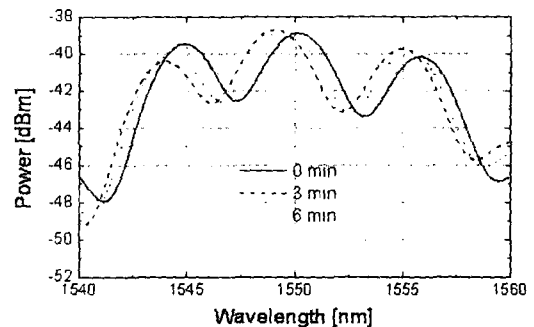

FIG. 10. Transmission spectra of the conventional unbalanced MZI measured at several times.
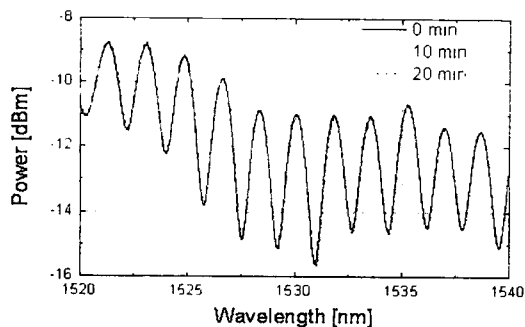
FIG. 11. Variation in transmission spectrum of the WDAI.

FIG. 12. Magnitude variation in the WDAI when no perturbation is applied to the sensor grating at 500 Hz.

strate thermal stability, we measured the transmission spectrum of our device every ten minutes during 1 hour. The first three results are shown in Fig. 11 and the phase drift or any variation in spectrum is rarely found. In the conventional MZI, the light split by a 3 dB coupler propagates in two arms and may experience quite different physical environments such as ambient temperature. In the proposed device, however, the interference fringes originate from the phase difference produced by the mismatch in refractive index of core and cladding in *the same* fiber with tens of centimeters, and lights propagating along the two 'arms' experience nearly the same condition even in ambient temperature change.

To quantify this thermal characteristic, we measured the lock-in amplifier outputs (amplitude of signal at the frequency of the applied serrodyne modulation) versus time when no perturbation is applied to the sensor grating at the frequency of 500 Hz. The amplitude variation was suppressed as less than 0.13 mV in this case during the measurement time (See Fig. 12.). If we define a figure of merit as *measurement range / maximum variation in measurand*, the value is 360 [14] in a typical unbalanced MZI with a reference grating and 461 in the proposed device.

V. CONCLUSION

We have introduced the WDAI and demonstrated its successful application in FBG sensor system to monitor a fine wavelength shift with prominent stability. Experimental results confirm that this technique can be employed to detect small wavelength shift of FBG sensor with high resolution and stability. This device has the outstanding performance in both resolution and stability among the interrogation techniques that have been suggested and demonstrated to date. The proposed device features negligible thermal
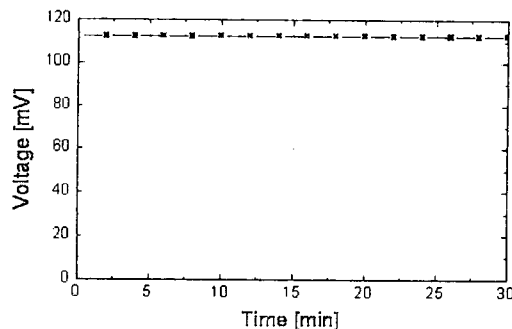
drift in transmission spectrum. The wavelength resolution is 0.05 pm in quasi-static measurement which corresponds to nearly 41.7 nϵ and 3.8×10^{-3} °C with sensitivities of 1.2 pm/$\mu\epsilon$ and 13 pm/°C. For the measurement of dynamic strain, the minimal detectable signal was 98.3 p$epsilon$ (rms)/Hz$^{1/2}$ at 100 Hz without modulation of pump LD and 8.76 n$epsilon$/Hz$^{1/2}$ at 100 Hz dynamic strain with pump LD modulation of 5 kHz. The WDAI will emerge as a significant device to monitor fine Bragg wavelength shift with great thermal stability that can measure both quasi-static measurands and dynamic ones provided that the modulation frequency is suitably chosen considering the applied perturbation.

*Corresponding author : byoungho@plaza.snu.ac.kr.

REFERENCES

[1] M. A. Davis and A. D. Kersey, Electron. Lett. **30**, 75 (1994).
[2] A. D. Kersey, T. A. Berkoff, and W. W. Morey, Opt. Lett. **18**, 1370 (1993).
[3] M. G. Xu, H. Geiger, J. L. Archambault, L. Reekie, and J. P. Dakin, Electron. Lett. **29**, 1510 (1993).
[4] A. D. Kersey, T. A. Berkoff, and W. W. Morey, Electron. Lett. **28**, 236 (1992).
[5] J. Jung, Y. W. Lee, and B. Lee, Proc. SPIE, 4185, 114 (2000).
[6] J. Jung, Y. W. Lee, and B. Lee, in The 13th Annual IEEE Lasers and Electro Optics Society Meeting (LEOS) (Rio Grande, Puerto Rico, USA, 2000), 679.
[7] D. P. Hand and P. St. J. Russel, Opt. Lett., **15**, 102 (1990).
[8] E. M. Dianov, S. A. Vasiliev, A. S. Kurkov, O. I. Medvedkov, and V. N. Protopopov, in Proc. Of European Conf. on Optical Communication (Gent, Belgium, 1997), 65.

[9] B. H. Lee and J. Nishii, Opt. Lett. **23**, 1624 (1998).

[10] D. S. Starodubov, V. Grubsky, and J. Feinberg, IEEE Photon. Technol. Lett. **10**, 1590 (1998).

[11] Y. Jeong, S. Baek, and B. Lee, IEEE Photon. Technol. Lett. **12**, 1216 (2000).

[12] Y.-J. Rao, *Optical Fiber Sensor Technology* (Chap-

man & Hall, London, UK, 1998) vol. 2.

[13] A. D. Kersey, T. A. Berkoff, and W. W. Morey, Opt. Lett. **18**, 72 (1993).

[14] M. Song, Ph. D. dissertation, Seoul National University (1997).